

Overestimated Arctic warming and underestimated Eurasia mid-latitude warming in CMIP5 simulations

Yongkun Xie, Yuzhi Liu and Jianping Huang*

Key Laboratory for Semi-Arid Climate Change of the Ministry of Education, College of Atmospheric Sciences, Lanzhou University, China

ABSTRACT: The surface air temperature (SAT) trends from historical simulations of the Coupled Model Intercomparison Project Phase 5 (CMIP5) were compared with observations for the period of 1955–2004. The observed spatial pattern of SAT trends was strikingly different from the CMIP5-historical simulations over mid- and high-latitude Northern Hemisphere. The strongest observed warming for the Eurasian Continent was over mid latitudes. However, the CMIP5 historical simulations indicated enhanced warming over higher latitudes, and the warming trends increased from low to higher latitudes. The zonal mean SAT trends indicated overestimated warming in high-latitude and underestimated warming in mid-latitude land over Northern Hemisphere in CMIP5 historical simulations, which resulted in opposite trends in the meridional temperature gradient over high latitudes compared with observations. The overestimated Arctic and underestimated Eurasia mid-latitude warming only occurred in cold season. Further comparison of the results of CMIP5 models from the Atmospheric Model Intercomparison Project and historical simulations revealed that model bias in sea surface temperature and the exaggerated response of temperature change to Arctic sea ice decline are possible reasons for poorly simulated Arctic and Eurasia mid-latitude temperature change.

KEY WORDS temperature trend; CMIP5; Arctic; model bias

Received 16 September 2014; Revised 30 November 2015; Accepted 6 December 2015

1. Introduction

The global mean temperature has increased by 0.74 °C from 1906 to 2005 (Trenberth *et al.*, 2007). As the global surface air temperature (SAT) rises, the rate of regional warming is not expected to be uniform across the globe or in different seasons (e.g. Fu *et al.*, 2006; Liu *et al.*, 2011; Jones *et al.*, 2012; Ji *et al.*, 2014; Huang *et al.*, 2015).

Enhanced and accelerated warming in the Arctic region, known as Arctic amplification (AA), has been observed during recent decades (Overland *et al.*, 2004; Wang and Overland, 2004; Pithan and Mauritsen, 2014). The AA occurs over the Arctic Ocean because of the loss of sea ice and infrared radiation feedback (Liu *et al.*, 2007; Screen and Simmonds, 2010; Bintanja and Van der Linden, 2013). However, the land surface undergoes larger temperature changes than those of the surrounding oceans in most latitude because of the different lapse rates between land and ocean in low-level troposphere (Joshi *et al.*, 2008). Huang *et al.* (2012) found that the warming trend was particularly enhanced over semi-arid regions in the cold season and reported a cold season mean SAT increase of 1.72 °C over semi-arid regions of Northern Hemisphere land (NHL). Wallace *et al.* (2012) suggested that the enhanced boreal wintertime warming was mainly dynamically induced and

noted an obvious discrepancy in the spatial pattern of SAT trends between observations and Coupled Model Intercomparison Project Phase 3 (CMIP3) simulations.

The Intergovernmental Panel on Climate Change (IPCC) has concluded that human activities such as the emission of greenhouse gases are the main cause of current global warming (IPCC, 2007). However, ocean processes and air–sea interactions also have an important role in surface temperature change; for example, the warming hiatus of the past decade is associated with ocean heat uptake in the Atlantic, Southern oceans, and tropical Pacific (Guemas *et al.*, 2013; Chen and Tung, 2014). Kosaka and Xie (2013) and England *et al.* (2014) also suggested that the warming hiatus is tied to equatorial Pacific surface cooling induced by accelerated Pacific trade winds. Additionally, changes in internal climate variability also have a significant influence on the global climate on a decadal to multi-decadal time scale. Thompson and Wallace (2000) argued that the observed change in the Arctic Oscillation during the last three decades of the 20th century significantly contributed to the warming trend over Eurasia and North America, accounting for 50% of the winter warming over Eurasia. Huang *et al.* (1998) proposed a link between the North Atlantic Oscillation and the El Niño Southern Oscillation (ENSO), which suggests that the coactions of internal climate variability can influence climate significantly. For high-latitude regions, ice/snow cover is an important feature. A change in ice/snow cover could strongly influence the local climate and also have

* Correspondence to: J. Huang, Key Laboratory for Semi-Arid Climate Change of the Ministry of Education, College of Atmospheric Sciences, Lanzhou University, 222 Tianshui Road, Lanzhou, 730000, China. E-mail: hjp@lzu.edu.cn

Table 1. Model simulations examined in this study.

Model name	Institute name
1. ACCESS1.0	CSIRO and Bureau of Meteorology, Australia
2. ACCESS1.3	CSIRO and Bureau of Meteorology, Australia
3. BCC-CSM1.1	Beijing Climate Center, China
4. BCC-CSM1.1(m)	Beijing Climate Center, China
5. CanESM2	Canadian Centre for Climate Modelling and Analysis, Canada
6. CCSM4	University of Miami - RSMAS, USA
7. CESM1(BGC)	Community Earth System Model Contributors, USA
8. CESM1(CAM5)	Community Earth System Model Contributors, USA
9. CESM1(FASTCHEM)	Community Earth System Model Contributors, USA
10. CESM1(WACCM)	Community Earth System Model Contributors, USA
11. CNRM-CM5	Centre National de Recherches Météorologiques, France
12. CNRM-CM5-2	Centre National de Recherches Météorologiques, France
13. CSIRO-Mk3.6.0	CSIRO in collaboration with QCCCE, Australia
14. FGOALS-g2	Institute of Atmospheric Physics, Tsinghua University, China
15. GFDL-CM2.1	NOAA Geophysical Fluid Dynamics Laboratory, USA
16. GFDL-CM3	NOAA Geophysical Fluid Dynamics Laboratory, USA
17. GFDL-ESM2G	NOAA Geophysical Fluid Dynamics Laboratory, USA
18. GFDL-ESM2M	NOAA Geophysical Fluid Dynamics Laboratory, USA
19. GISS-E2-H	NASA Goddard Institute for Space Studies, USA
20. GISS-E2-H-CC	NASA Goddard Institute for Space Studies, USA
21. GISS-E2-R	NASA Goddard Institute for Space Studies, USA
22. GISS-E2-R-CC	NASA Goddard Institute for Space Studies, USA
23. HadCM3	Met Office Hadley Centre, UK
24. HadGEM2-AO	Met Office Hadley Centre, UK
25. IPSL-CM5A-LR	Institut Pierre-Simon Laplace, France
26. IPSL-CM5A-MR	Institut Pierre-Simon Laplace, France
27. IPSL-CM5B-LR	Institut Pierre-Simon Laplace, France
28. MIROC-ESM	JAMSTEC, The University of Tokyo and NIES, Japan
29. MIROC-ESM-CHEM	JAMSTEC, The University of Tokyo and NIES, Japan
30. MIROC5	The University of Tokyo, NIES and JAMSTEC, Japan
31. MPI-ESM-LR	Max Planck Institute for Meteorology, Germany
32. MPI-ESM-P	Max Planck Institute for Meteorology, Germany
33. MRI-CGCM3	Meteorological Research Institute, Japan
34. MRI-ESM1	Meteorological Research Institute, Japan
35. NorESM1-M	Norwegian Climate Centre, Norway
36. NorESM1-ME	Norwegian Climate Centre, Norway
37. BNU-ESM	Beijing Normal University, China
38. EC-EARTH	EC-EARTH consortium, 10 European countries
39. FIO-ESM	The First Institute of Oceanography, SOA, China
40. INM-CM4	Institute for Numerical Mathematics, Russia
41. MPI-ESM-MR	Max Planck Institute for Meteorology, Germany

an impact on the global climate (Wang and Stone, 1980; Jeong *et al.*, 2011; Fletcher *et al.*, 2012; Lorant *et al.*, 2014).

In this study, the observed features of Northern Hemisphere warming were analysed and compared with the CMIP Phase 5 (CMIP5) simulation (Taylor *et al.*, 2012). Five different observed SAT data sets and the output from 41 CMIP5 models were used to ensure that the results were robust. The details of the data sets and the methodology used are given in Section 2. In Section 3, comparisons of observed changes in Northern Hemisphere SAT with CMIP5 historical simulations are presented from multiple perspectives, including a comparison between the warm (May to September) and cold seasons (November to March), land–sea contrasts, zonal mean features, and regional mean features in different latitudinal zones. Discussions and a summary are presented in Section 4.

2. Data sets and methods

2.1. Data sets

The SAT data from the GISS Surface Temperature Analysis (GISTEMP), Merged Land–Ocean Surface Temperature (MLOST) analysis data set, HadCRUT4 data set, Climatic Research Unit (CRU), and GHCN-M data set were analysed in this study. The GISTEMP data set from the National Aeronautics and Space Administration Goddard Institute for Space Studies (GISS) has a resolution of $2^\circ \times 2^\circ$ and covers the period from 1880 to the present day (Hansen *et al.*, 2010). The MLOST data set (version 3b) from the National Climate Data Center has a resolution of $5^\circ \times 5^\circ$ and covers the period from 1880 to 2010 (Smith *et al.*, 2008). The HadCRUT4 data set (version 4.2.0.0), provided by the Met Office Hadley Centre, covers the period from 1850 to the present day and has a resolution of $5^\circ \times 5^\circ$ (Morice *et al.*, 2012). The 100 ensemble members

of the HadCRUT4 were used to quantify observational uncertainty. The CRU data set (version TS3.10), provided by the University of East Anglia, covers the period from 1901 to 2009 and has a resolution of $0.5^\circ \times 0.5^\circ$ (Harris *et al.*, 2013). The GHCN-M data set (version 3.2.0) has a resolution of $5^\circ \times 5^\circ$ (Lawrimore *et al.*, 2011). Besides, the sea ice concentration (SIC) data from Met Office Hadley Centre's HadISST1 data set were also used (Rayner *et al.*, 2003).

The 41 CMIP5 models analysed in this study are listed in Table 1. We used the SAT data from CMIP5 historical and the Atmospheric Model Intercomparison Project (AMIP) simulations. Here, the CMIP5 simulation refers to the multi-model ensemble mean result of CMIP5 models. The result of each individual model was represented by the mean of all its available ensemble members. We also used the SIC data from CMIP5 historical simulations. The SIC data are only available for the first 36 models as listed in Table 1.

2.2. Methods

To clearly present the features of SAT change, the linear trend of SAT was first calculated for the period 1955–2004. The CMIP5 historical simulation is generally from 1850 to 2005, and the cold season is from November to the following March (e.g. the 1955 cold season is from November 1955 to March 1996), so we chose the 2004 as the study end. The analysis was conducted from 1955, because the five observation data sets have little missing data from 1950 onward, and 1955–2004 can be easily divided into five decades to calculate decadal average SAT anomalies. Based on the annual and seasonal SAT anomalies for 1955–2004, the temporal series of regional mean SAT anomalies over low- (0° – 30° N), mid- (30° – 60° N), and high-latitude (60° – 90° N) zones were calculated separately for land, ocean, and the globe, respectively.

To compare the contribution of each latitude zone (k) to the mean SAT trend of NHL, we calculated the contribution rate (CR_k) of latitude zone k (Huang *et al.*, 2012):

$$CR_k = \frac{a_k \cdot \sum_{i=1}^{N_k} W_{ki}}{A_g \cdot \sum_{i=1}^{N_g} W_{ki}} \quad (1)$$

where a_k is the mean SAT trend for region k , $W_{ki} = \cos(\theta_i \cdot \pi/180.0)$, θ_i is the latitude of grid i , N_k is the number of grids in region k , A_g is the mean SAT trend of NHL, and N_g is the total number of all grids over NHL.

3. Results of the analysis

Based on the MLOST data set, we presented the zonal mean SAT trends over land, ocean, and the globe. Figure 1 shows the zonal mean SAT trends for 1955–2004. The

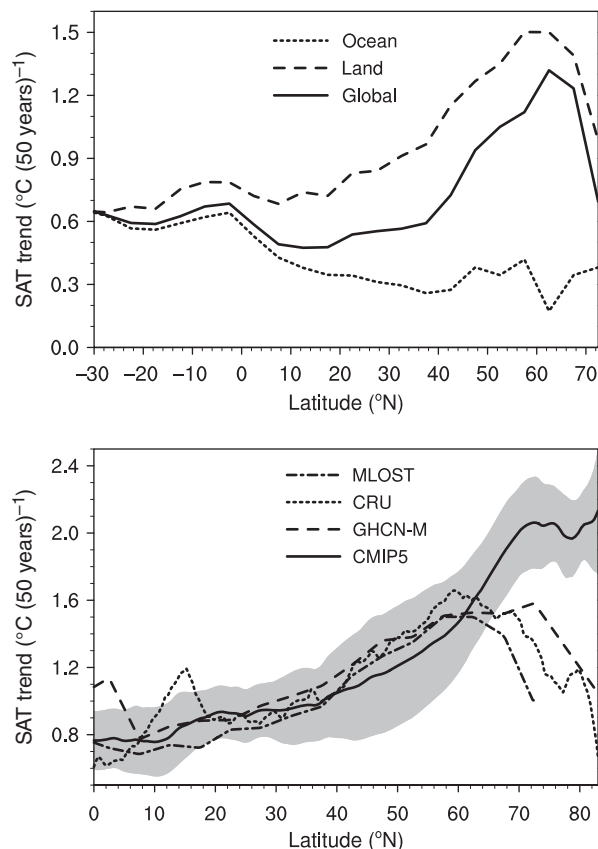


Figure 1. Zonal mean of annual SAT trends expressed in units of $^\circ\text{C} (50 \text{ years})^{-1}$ for the period of 1955–2004. (a) Observations over the globe (solid line), land (dashed line), and ocean (dotted line) based on MLOST data set. (b) Observations over land based on the MLOST (dotted-dashed line), CRU (dotted line) and GHCN-M (dashed line) data sets, and historical simulations by CMIP5 models (solid line) with standard deviations (grey shaded areas).

zonal mean SAT increased at all latitudes, and the warming over land was greater than that over ocean (Figure 1(a)). The trend for SAT to warm over land increased significantly from 30° to 60°N , but then decreased at higher latitudes, with a similar distribution of SAT trends over the globe. The warming peaks are about 1.5 and 1.3°C at approximately 60°N over land and the globe, respectively. However, the SAT trends over the ocean are different, with the strongest warming being only 0.6°C .

Focusing on the marked warming trend over land (Figure 1(a)), we analysed the SAT trends over land based on the CRU and GHCN-M data sets for comparison with MLOST data and CMIP5 historical simulations (Figure 1(b)). Figure 1(b) suggests that the distribution of zonal mean SAT trends for CRU and GHCN-M are similar to those for MLOST. However, a discrepancy between observations and CMIP5 simulations appears over the continents poleward of 60°N . The CMIP5 simulations show a continuing trend towards enhanced warming from 60°N towards the pole over NHL, which means that the CMIP5 historical simulations overestimated high-latitude NHL warming compared with observations.

The spatial map of SAT trends over the NH, corresponding to Figure 1, is shown in Figure 2. Figure 2(a)–(c)

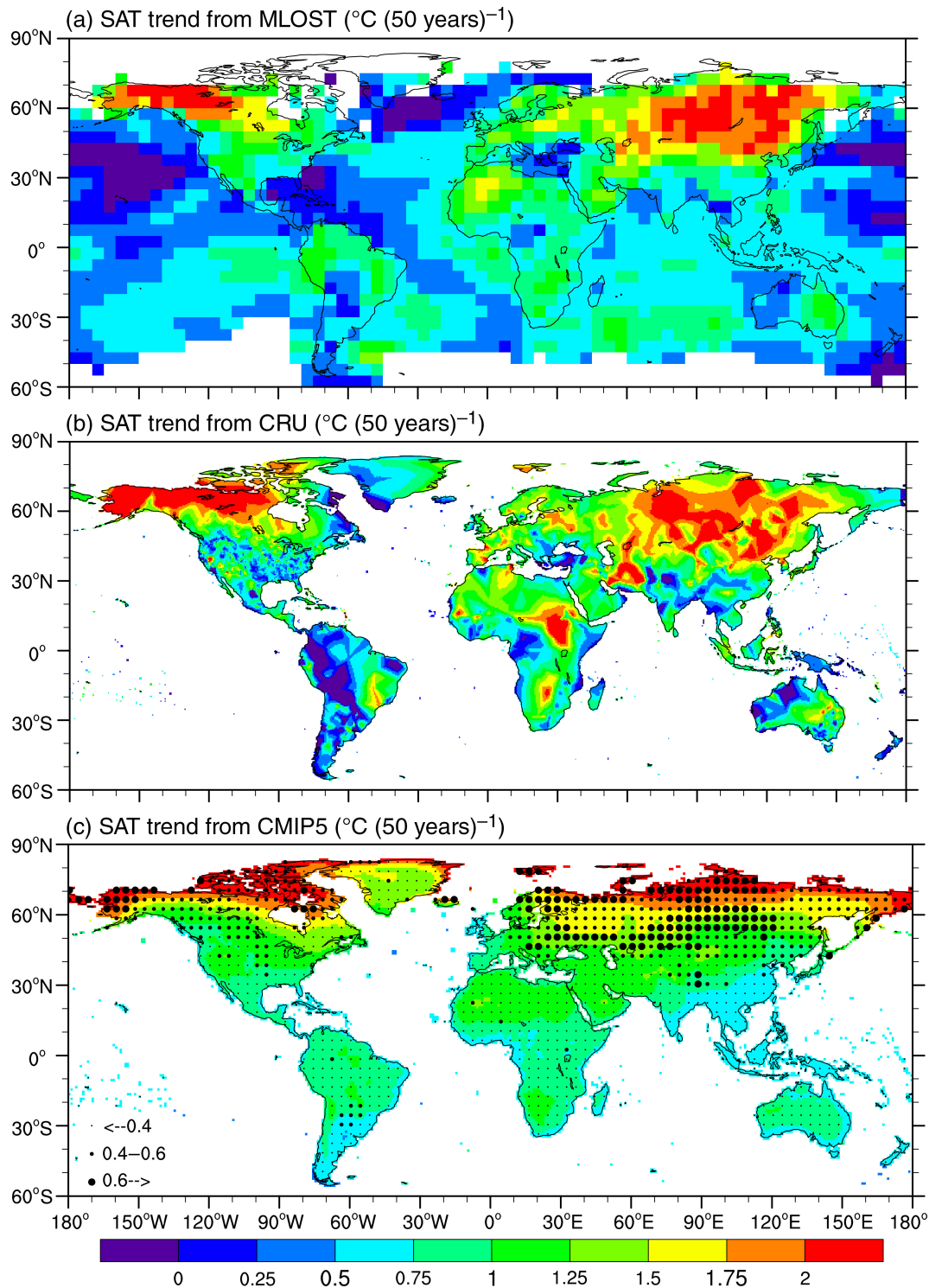


Figure 2. Annual mean SAT trends for 1955–2004 from (a) MLOST data, (b) CRU data, and (c) the multi-model ensemble mean of CMIP5 historical simulations. The black dots indicate the standard deviations of CMIP5 simulations, and the size of each dot indicates the magnitude of the standard deviation.

shows the SAT trends from MLOST data, CRU data, and CMIP5 historical simulations, respectively. In Figure 2(c), the standard deviations of CMIP5 models are denoted by the black dots, with the size of the dot indicating the magnitude of the standard deviation. As shown in Figure 2(a) and (b), the pattern of SAT trends over the NHL given by MLOST and CRU data is in

good agreement. The largest warming is observed over Eurasia and the northwest of North America (Figure 2(a) and (b)). However, the distribution of SAT trends from CMIP5 simulations is very different from the observations. The CMIP5 models did not simulate the enhanced warming over Eurasia (Figure 2(c)). Figure 2 also shows that, compared with observations, the CMIP5 simulations

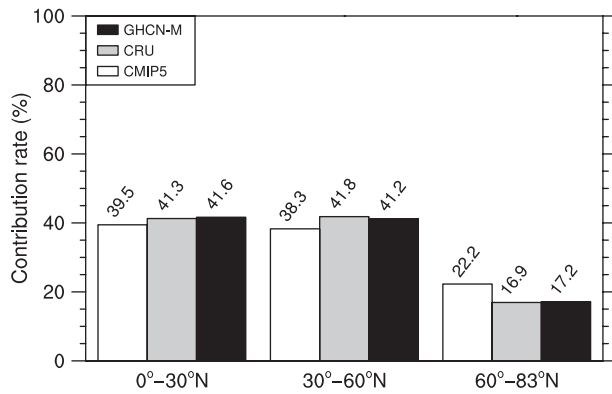


Figure 3. Proportional contribution of the regional mean SAT trends over low-latitude (0° – 30° N), mid-latitude (30° – 60° N), and high-latitude (60° – 83° N) areas to the mean SAT trends over NHL for the period of 1955–2004 using CRU data, GHCN-M data, and CMIP5 historical simulations.

clearly overestimated the warming over NHL at high latitudes. This overestimation of warming was mainly noted in the coastal areas over the high latitudes of Eurasia (Figure 2(c)). The spatial map of the SAT trends for 1979–2004 shows the same feature (Figure 9). Wallace *et al.* (2012) showed similar results for CMIP3 historical simulations.

Figure 3 shows the proportional contribution of regional mean SAT trends at low latitudes (0° – 30° N), mid-latitudes (30° – 60° N), and high latitudes (60° – 83° N) to the mean SAT trends over NHL using CRU data, GHCN-M data, and CMIP5 historical simulations. It can be seen that the contributions of the SAT trends over low and mid latitudes are greater than the contribution over high latitudes, and the results from two sets of observations are almost the same. The contributions from CMIP5 simulations over low- and mid-latitude regions are 2.0 and 3.2% lower than those from observations (mean of CRU and GHCN-M), respectively, but 5.2% higher than observations over high latitudes (Figure 3), which also indicates that the high latitudes have the largest model bias in the simulation of changes in SAT.

In addition to this bias, the overestimated warming over high-latitude NHL in CMIP5 historical simulations could also result in a discrepancy in meridional temperature gradient (MTG) trends between CMIP5 and observations. Figure 4 shows the trends in zonal mean MTG over NHL based on the CRU data set and CMIP5 historical simulations. A positive MTG in Figure 4 indicates an increase in the MTG, and a negative value indicates a decrease in the gradient. Figure 4 shows that the zonal mean MTG from CMIP5 simulations decreases over mid- and high-latitude continents as a result of the spatial pattern of the simulated SAT trends (Figure 2(c)). However, the observed MTG has the opposite sign at high latitudes compared with CMIP5 simulations. There will be stronger zonal wind and weaker planetary wave amplitude, when the MTG is stronger (Hassanzadeh *et al.*, 2014). The cold air from Arctic is more difficult to invade mid latitude, when there are stronger zonal winds and weakened planetary waves in

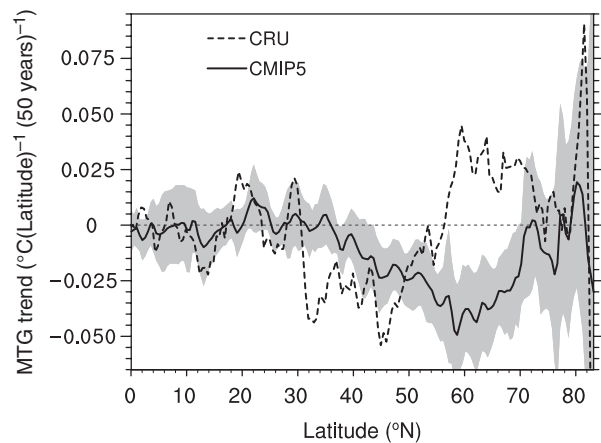


Figure 4. Annual mean meridional temperature gradient (MTG) trends in NHL expressed in units of $^{\circ}\text{C}(\text{degree latitude})^{-1} (50 \text{ years})^{-1}$ for the period of 1955–2004. The dashed and solid lines are observations based on CRU data and historical simulations by the CMIP5 models, respectively. The grey shaded areas denote standard deviations of CMIP5 simulations.

mid-high latitude. So the NH mid latitude will be warmer when MTG becomes stronger, and a warmer mid latitude will induce the MTG even stronger. This positive feedback is a possible reason of the enhanced mid-latitude warming (He *et al.*, 2014). Thus, the failure of CMIP5 models to simulate the enhanced mid-latitude terrestrial warming may be partly due to wrong simulations of this positive feedback.

Figure 5 shows the details of the change in NH SAT over different regions (land, ocean, and the globe) and different seasons [boreal warm season (May to September) and cold season (November to March)] by presenting the zonal mean SAT trends for 1955–2004. Three observation data sets were used in Figure 5. As shown in Figure 5(a) and (b), for low- and mid-latitude regions, the observed and simulated global mean SAT trends are almost identical. However, there is a huge difference over high latitudes in the cold season (Figure 5(c)). Although there are discrepancies among the observation data sets due to missing data, in all three data sets, the zonal mean SAT trend from CMIP5 historical simulations is significantly greater than the observed trend over high latitudes in the cold season. It can be seen from Figure 5(c) that the global mean SAT trend for the cold season increases substantially from 30° to 60° N and reaches a peak at about 60° N before decreasing at high latitudes. However, in contrast to these observations, the CMIP5 simulation indicated a consistent increasing trend of up to $2.5^{\circ}\text{C} (50 \text{ years})^{-1}$ in the cold season (Figure 5(c)).

As shown in Figure 5(d)–(f), the observed SAT trends over land for the cold season were very different from the CMIP5 simulated trends, and which for the warm season is more consistent with CMIP5 simulations. Compared with the observations, CMIP5 historical simulations overestimated the warming trend over high-latitude land and underestimated the warming trend over mid-latitude land in the cold season (Figure 5(f)). As for the SAT trends over ocean (Figure 5(g)–(i)), the simulated trend from CMIP5 is larger than observations from low to high latitude, and

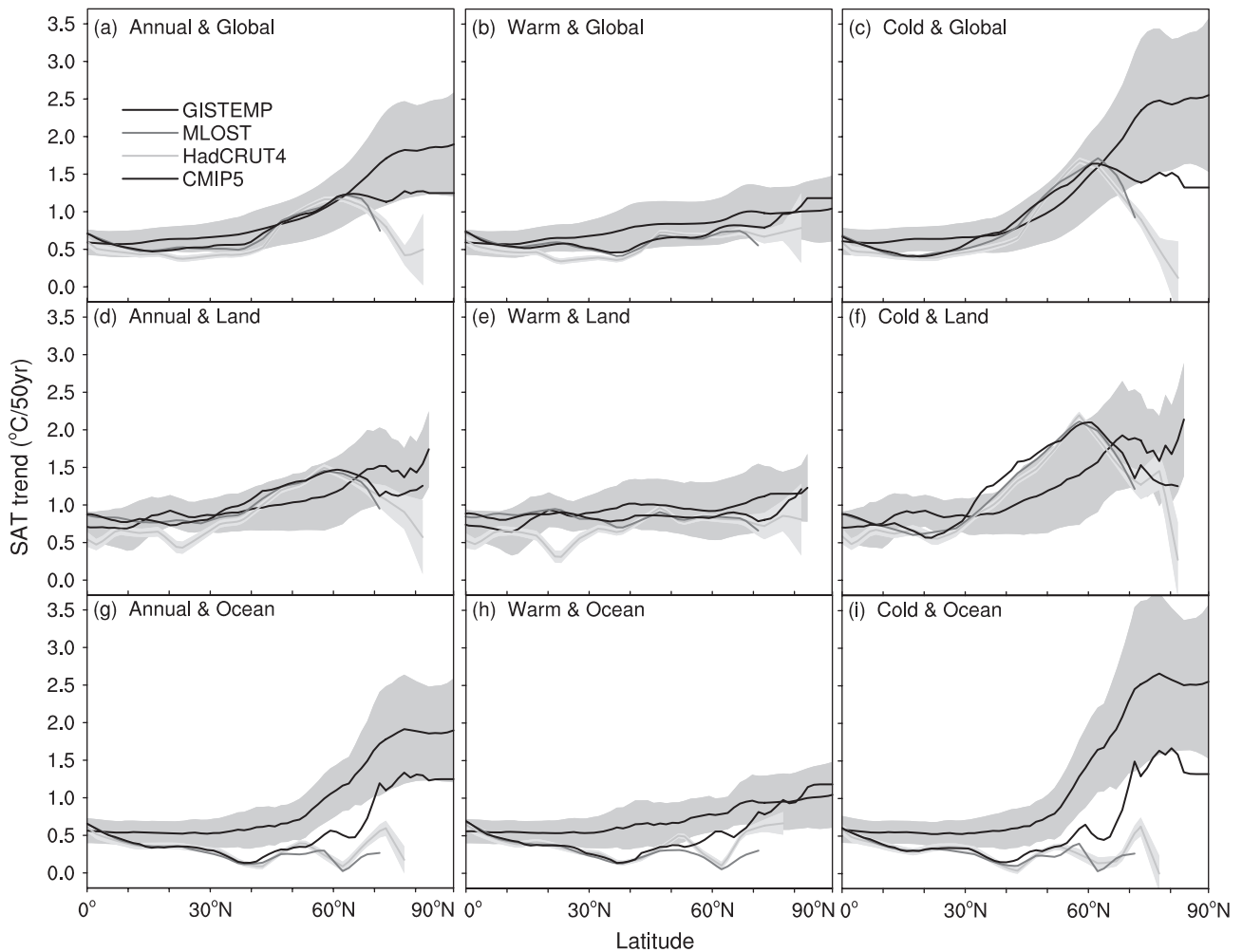


Figure 5. Zonal mean SAT trends expressed in units of $^{\circ}\text{C} (50 \text{ years})^{-1}$ for the period of 1955–2004. (a), (b), and (c) show the annual, warm season, and cold season mean SAT trends over the globe, respectively. (e), (f), and (g) are the same as (a), (b), and (c) but over land; (g), (h), and (i) are the average trends over ocean. The red, blue, and green lines are observations based on GISTEMP, MLOST, and HadCRUT4 data, respectively. The black line is the multi-model ensemble mean of CMIP5 models from the historical simulation, and the grey shading denotes one standard deviation of the CMIP5 simulations. The turquoise shading denotes one standard deviation of the 100 realizations from the HadCRUT4 data set.

which was most significant over the polar area during the cold season.

Figure 6 shows spatial maps of the SAT trends in boreal warm (left column) and cold seasons (right column) for 1955–2004. The cross, open circle, and filled circle indicate the standard deviations. The most significant warming can be seen to have occurred in the cold season in both the simulation and observations. As shown in Figure 6(a)–(f), the SAT trend derived from observations displays spatial inhomogeneity, with simultaneous occurrence of warming and cooling over the globe, although the trend is predominantly towards global warming. In contrast to observations, the CMIP5 historical simulations indicate a uniform warming trend over the globe, which just a forced warming signal responding to the external forcing – green house gas, solar radiation, and so on. Enhanced warming was observed over the Eurasian and North American continents in the cold season, as shown in Figure 6(b), (d), and (f). However, the CMIP5 simulations did not reconstruct the notable warming over the Eurasian and North American continents for the cold season. As presented in Figure 6(h),

the most obvious warming in the cold season according to the CMIP5 simulations occurs over the Arctic Ocean, and the warming becomes weaker from the pole to the equator. To support the results shown by the linear trend of SAT, we also analysed the SAT anomalies for every decade during 1955–2004 (Figure S1, Supporting Information). As shown in Figure S1, the evolution of SAT anomalies during these three intervals further confirms the result shown in Figure 6. The simulated distribution of SAT anomalies during these three periods was clearly different from the observations.

Figure 7 shows the simulated and observed SAT anomalies for 1950–2004 relative to 1961–1990 over the land averaged from 0° to 30°N , from 30° to 60°N , and from 60° to 90°N . Figures 7(a)–(c), (d)–(f), and (g)–(i) show annual, warm season, and cold season data, respectively. Figure 8 is same as Figure 7 but for ocean. The most remarkable difference between the observed and simulated mid-latitude SAT anomalies over land occurred in the cold season (Figure 7(e) and (h)). The annual series of SAT anomalies show that the observed warming over

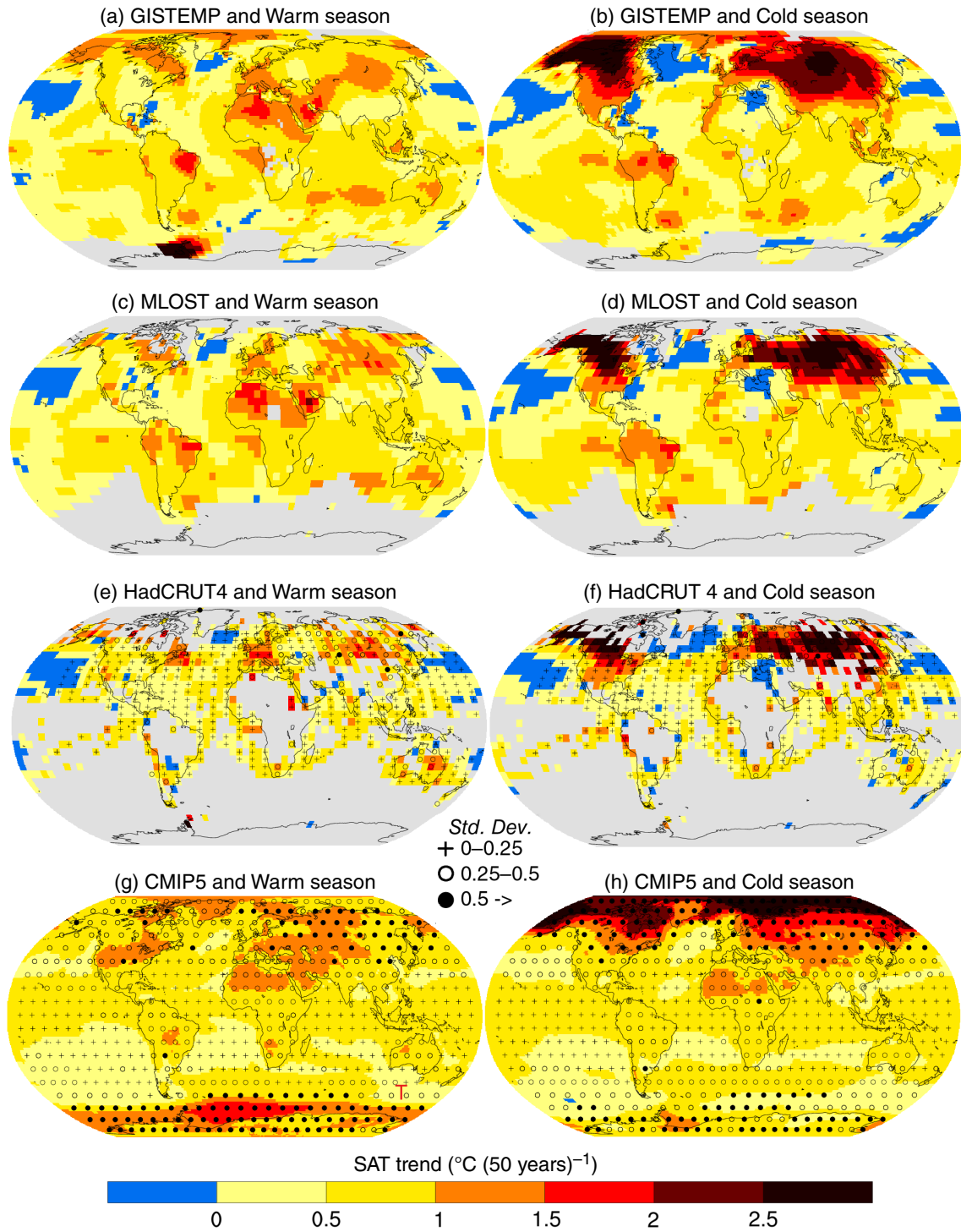


Figure 6. Trend in global SAT for the period of 1955–2004 from (a), (b) GISTEMP data; (c), (d) MLOST data; (e), (f) HadCRUT4 data; and (g), (h) the multi-model ensemble mean of CMIP5 models from the historical simulation. The left-hand column is for the warm season, and the right-hand column is for the cold season. Black symbols in (e), (f) and in (g), (h) denote one standard deviation of the 100 realizations from the HadCRUT4 data set and the CMIP5 simulations, respectively. Grey areas indicate incomplete or missing data.

mid-latitude land is greater than in the CMIP5 simulations in the cold season (Figure 7(h)). Figure 8 suggests that the observed SAT anomalies over low-latitude ocean were consistent with the CMIP5 simulations. As shown in Figures 8(e) and (h), the observed SAT trends over the mid-latitude ocean were smaller than the CMIP5 simulations for both the warm and cold seasons. In high-latitude

ocean areas, the MLOST and HadCRUT4 data sets had many missing values, which generated huge differences among the three observation data sets. Figure 8(a) shows that the observed warming trend was smaller than in the CMIP5 simulations over high-latitude ocean, as indicated by the trend in both the annual and decadal averages. Same as Figure 7, the global mean results are shown

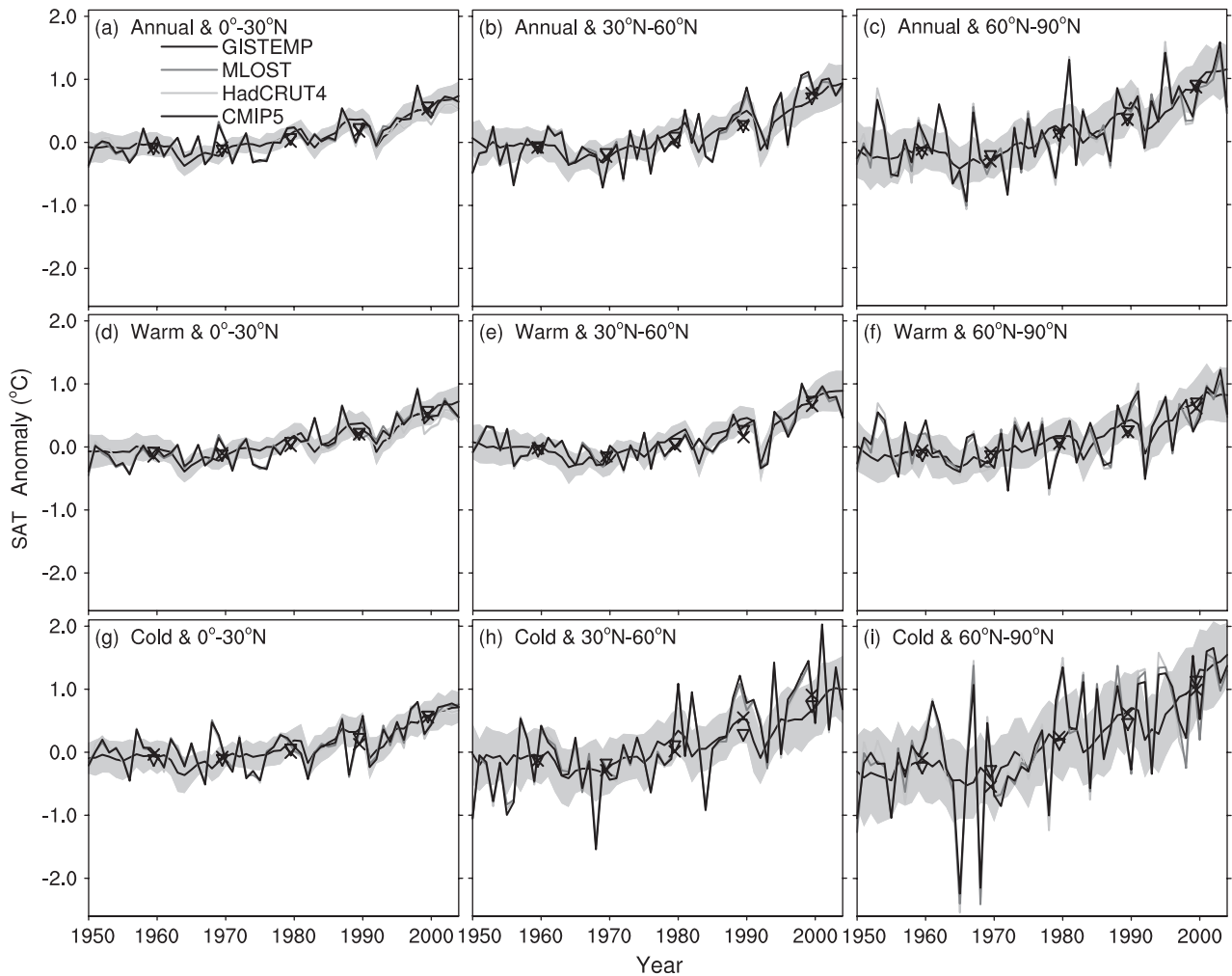


Figure 7. Temporal series of SAT anomalies over the land relative to 1961–1990 climatology expressed in units of °C for the period of 1950–2004. (a), (b), and (c) are the annual mean; (d), (e), and (f) are the warm season; and (g), (h), and (i) are the cold season. The left, middle, and right columns are averaged over the region from 0° to 30°N, 30° to 60°N, and 60° to 90°N over the globe, respectively. Red, blue, green, and black lines are observations based on GISTEMP, MLOST, and HadCRUT4 data sets and the multi-model ensemble mean of CMIP5 models from the historical simulation, respectively. The turquoise and grey shading denote one standard deviation of 100 realizations from the HadCRUT4 data set and the CMIP5 models, respectively. Orange symbols (x, v) denote the mean of every decade during the period of 1955–2004 from the mean of three observations and the multi-model ensemble mean of the CMIP5 models, respectively.

in Figure S2. Compared with the observations, CMIP5 historical simulations displayed weak year-to-year fluctuation because of the smoothing that resulted from averaging many models. The clear year-to-year fluctuation observed in the cold season was mainly induced by dynamic processes (Wallace *et al.*, 2012).

To examine the model bias induced by interactions among air, sea, and sea ice, the results of AMIP simulations were compared with historical simulations. Figure 9 shows SAT trends for the period of 1979–2004, in which the AMIP simulation prescribes the observed sea surface temperature and sea ice for 1979 to present day (Taylor *et al.*, 2012). Compared with the results from the CMIP5 historical simulation, the results from the AMIP simulation were more consistent with the observations. The AMIP simulations did not produce the overestimated Arctic warming previously identified in the CMIP5 historical simulations (Figure 9(h), and (f)). So the overestimated high-latitude warming and underestimated mid-latitude warming were

probably connected with the Arctic sea ice and sea surface temperature.

As the NH high latitude has largest internal variability in CMIP5 models (Figure S3), the Arctic sea ice and sea surface temperature appear to be key factors in simulating the SAT over NH high latitudes. As shown in Figure 10, the larger decline rate of Arctic SIC was corresponding to a larger Arctic warming trend for boreal cold season in CMIP5 models. So the Arctic sea ice decline is connected with the AA in CMIP5 models, and the SIC in autumn and early winter were more correlated with the AA (Figure 10). Compared with observations, most of the models simulated weaker decline trends of Arctic sea ice in the months except October and November (Figure 10). However, the warming amplitudes responding to the sea ice decline in the models were obviously stronger than observations (Figure 10). Thus, the exaggerated response of temperature change to the Arctic sea ice decline was partly responsible to the overestimated Arctic

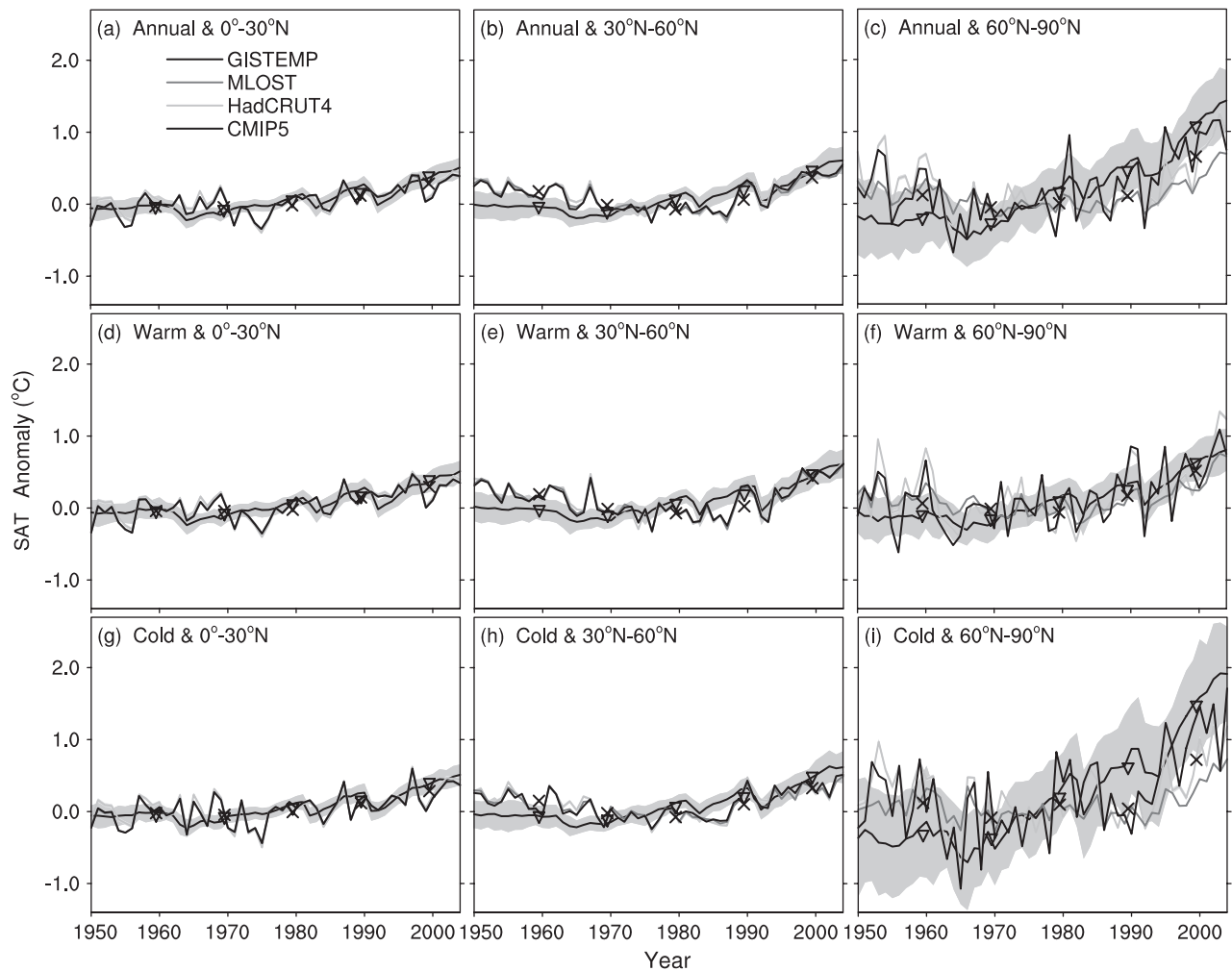


Figure 8. Same as Figure 7 but for the average over ocean.

warming in CMIP5 models. Besides the local influence on high-latitude temperature, the Arctic sea ice also has significant influence on mid-latitude temperature through its effect on atmospheric circulation variability, e.g. polar vortex, planetary waves, Arctic Oscillation, and so on (Cohen *et al.*, 2014; Mori *et al.*, 2014). The ‘warm arctic and cold Eurasia’ pattern were also presented in many climate models (Mori *et al.*, 2014), so the exaggerated response of the temperature change to the Arctic sea ice decline may also correlate with underestimated mid-latitude warming.

4. Summary and discussion

CMIP5 historical simulations clearly overestimated the trend for increasing annual SAT over Arctic regions. Additionally, the CMIP5 models did not simulate the enhanced warming over Eurasia, and overestimated the warming trend in the coastal areas over the high-latitude regions of Eurasia. The contributions of the regional mean to the NHL mean SAT trends from CMIP5 historical simulations over low- and mid-latitude regions were 2.0 and 3.2% lower than observation, respectively, but they were 5.2% higher than observations at high latitudes. The zonal mean MTG

from CMIP5 historical simulations decreased in the mid and high latitudes over NHL, but the observed MTG trend displayed the opposite sign at high latitudes compared with CMIP5 simulations. The failure of CMIP5 models to simulate the positive feedback associated zonal circulation, planetary wave amplitude, and MTG is a possible reason for underestimated Eurasia mid-latitude warming.

The overestimated Arctic and underestimated Eurasia mid-latitude warming by CMIP5 only occurred in the boreal cold season. The largest internal variability in the CMIP5 models also occurred over NH high latitude in the boreal cold season, especially over the Arctic Ocean near Greenland and Eurasia. Compared with the results from the CMIP5 historical simulation, the results from the AMIP simulation were more consistent with observations. The AMIP simulations better simulated the SAT change over Eurasian continents especially for the warm season, and did not produce overestimated Arctic warming. So the Arctic sea ice and sea surface temperature appear to be key factors in simulating the pattern of SAT change over NHL and Arctic.

The Arctic sea ice decline is connected with the AA in CMIP5 models, and the sea ice decline was weaker than observations for most models. However, the warming

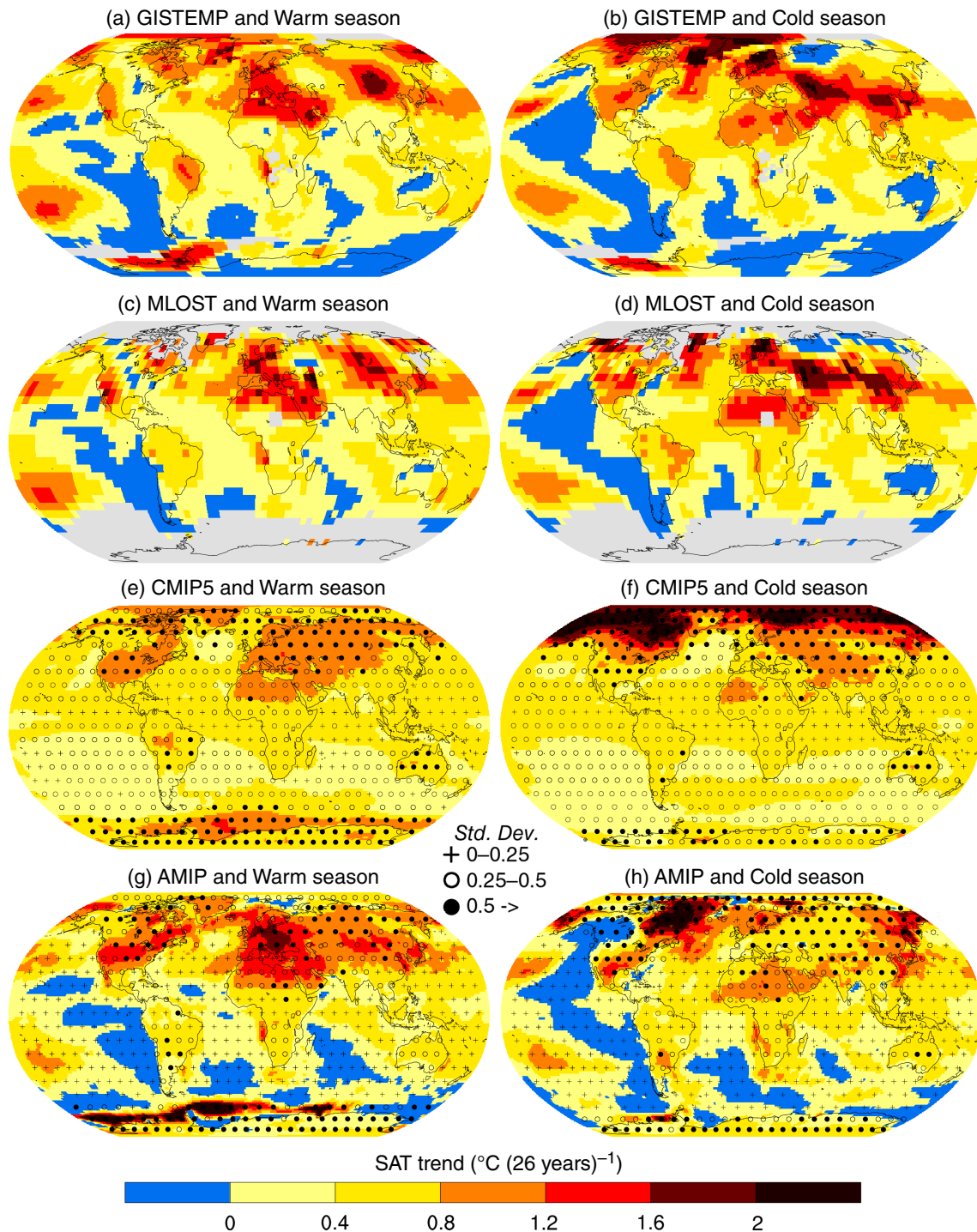


Figure 9. Trend in global SAT for the period of 1979–2004 from (a), (b) GISTEMP data; (c), (d) MLOST data; (e), (f) the multi-model ensemble mean of CMIP5 models from the historical simulation; and (g), (h) the multi-model ensemble mean of CMIP5 models from the AMIP simulation. The left-hand column is the warm season, and the right-hand column is the cold season. Black symbols in (e), (f), (g), and (h) denote one standard deviation of the CMIP5 models. Grey areas indicate incomplete or missing data.

amplitudes responding to the sea ice decline in the models were obviously exaggerated than observations. So the exaggerated response of temperature change to Arctic sea ice decline was responsible to the overestimated Arctic warming rather than the larger decline trends of sea ice in CMIP5 models. Besides, the Arctic sea ice may also correlate with underestimated mid-latitude warming in CMIP5 models through its effect on atmospheric

circulation variability (Mori *et al.*, 2014). However, as sea ice component and the coupling of it with other components in each CMIP5 models are different, the specific response of bias in Arctic sea ice and sea surface temperature for each individual model therefore requires further study.

The bias in the AMIP simulations in the cold season over Eurasia mid-latitude was still obvious compared with the

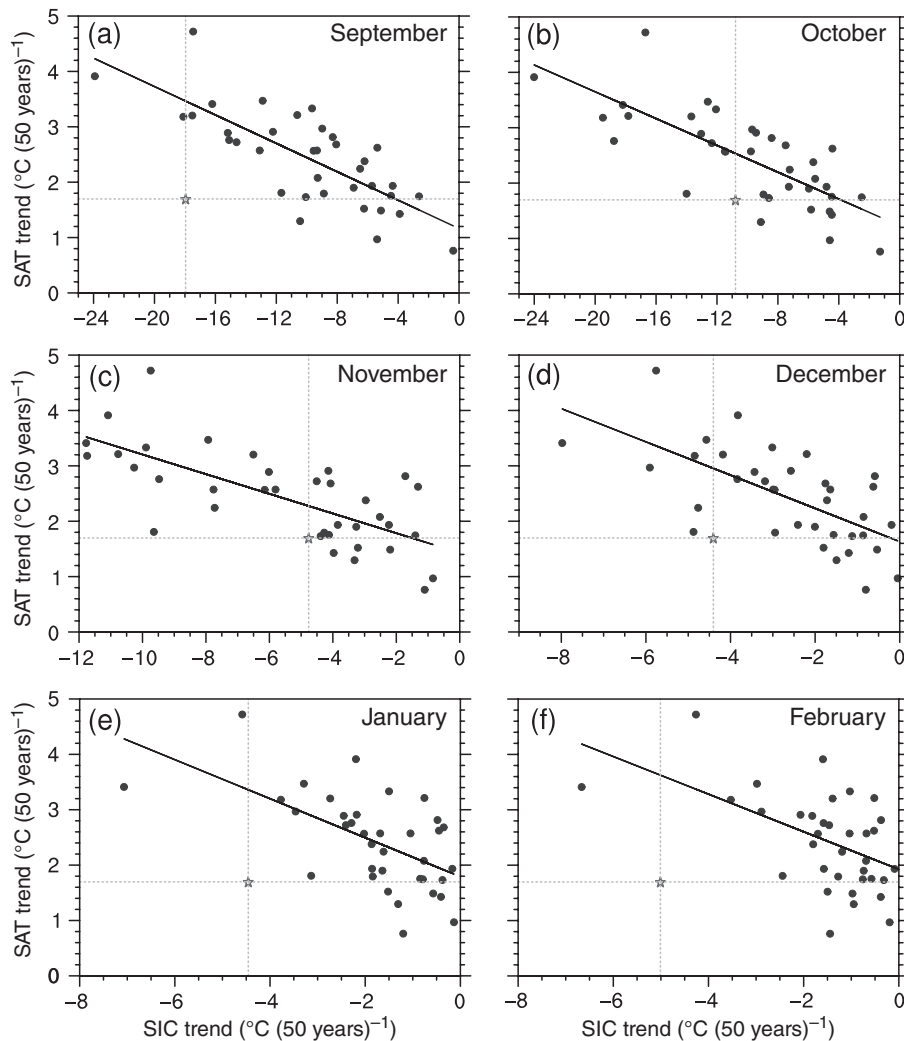


Figure 10. (a) Scatterplot of the linear trend from 1955 to 2004 in SAT averaged over 70°N poleward for boreal cold season as a function of the trend in sea ice concentration (SIC) averaged over 70°N poleward for September, every dot represents a result from one of the first 36 CMIP5 model as listed in Table 1. The pentagram represents the observed result from GISTEMP SAT data and HadISST1 SIC data. (b)–(f) Same as (a) but for SIC in different month.

warm season. Although the AMIP simulation forced by observed sea ice and sea surface temperature, the response of atmosphere to oceanic forcing and the internal atmospheric variability may also have some bias. As the Eurasia mid latitude was significantly influenced by internal circulation variability (Thompson and Wallace, 2000; Deser *et al.*, 2012; Wallace *et al.*, 2012; He *et al.*, 2014), the bias over Eurasia mid latitude in AMIP simulations may be partly induced by the internal atmospheric variability. Additionally, in the historical simulation experiment, the CMIP5 models showed some weaknesses in simulating internal climate variability (Taylor *et al.*, 2012). This defect in the CMIP5 models in simulating internal climate variability may also induce some bias in the NH mid- and high-latitude SAT trend, especially when the modes of internal climate variability in observations have long-term monotonic trends or stimulative coactions. Therefore, the modes of internal climate variability in the NH, such as the North Atlantic Oscillation (Higuchi *et al.*, 1999; Shabbar *et al.*, 2001; Huang *et al.*, 2006), Arctic

Oscillation (Li *et al.*, 2014), and Pacific Decadal Oscillation (McCabe *et al.*, 2012), should also be examined in both CMIP5 models and observations.

Acknowledgements

We thank Yi Ming for useful discussions and suggestions. We acknowledge the Program for Climate Model Diagnosis and Intercomparison and the World Climate Research Programme's Working Group on Coupled Modelling, which is responsible for CMIP. We also thank the climate modelling groups for producing and making their available model output. This research was jointly supported by the National Basic Research Program of China (2012CB955301), National Natural Science Foundation of China (41475095), Program for Changjiang Scholars and Innovative Research Team in University (PCSIRT), the Fundamental Research Funds for the Central Universities (lzujbky-2013-ct05, lzujbky-2014-109, and lzujbky-2009-k03), and China 111 project (B13045).

Supporting Information

The following supporting information is available as part of the online article:

Figure S1. Anomalies in global surface air temperature (SAT) relative to 1961–1990 climatology for the decadal mean of (a), (d), (g), (j), 1955–1964; (b), (e), (h), (k), 1975–1984; and (c), (f), (i), (l), 1995–2004. The first and third rows are observations based on GISS Surface Temperature Analysis (GISTEMP) data and show results for the warm and cold seasons, respectively. The second and fourth rows are multi-model ensemble means of Coupled Model Intercomparison Project Phase 5 (CMIP5) models from historical simulations and show the results of warm and cold seasons, respectively. The black symbols in the second and fourth rows denote one standard deviation of the CMIP5 models, whose value is the same as in Figure 6. Grey areas indicate incomplete or missing data.

Figure S2. Temporal series of surface air temperature (SAT) anomalies over the globe relative to 1961–1990 climatology expressed in units of °C for the period of 1950–2004. (a), (b), and (c) are the annual mean; (d), (e), and (f) are the warm season; and (g), (h), and (i) are the cold season. The left, middle, and right columns are averaged over the region from 0° to 30°N, 30° to 60°N, and 60° to 90°N over the globe, respectively. Red, blue, green, and black lines are observations based on GISS Surface Temperature Analysis (GISTEMP), Merged Land–Ocean Surface Temperature (MLOST), and HadCRUT4 data sets and the multi-model ensemble mean of Coupled Model Intercomparison Project Phase 5 (CMIP5) models from the historical simulation, respectively. The turquoise and grey shading denote one standard deviation of 100 realizations from the HadCRUT4 data set and the CMIP5 models, respectively. Orange symbols (×, ∇) denote the mean of every decade during the period of 1955–2004 from the mean of three observations and the multi-model ensemble mean of the CMIP5 models, respectively.

Figure S3. One standard deviation of the detrended surface air temperature (SAT) from the historical simulation of 41 Coupled Model Intercomparison Project Phase 5 (CMIP5) models averaged for the period of 1955–2004. (a), (b), and (c) are for annual, warm season, and cold season, respectively. Note that firstly the SAT from each model was detrended by removing their linear trends for 1955–2004. Then the one standard deviation of the detrended SAT for 1955–2004 from each model was calculated, separately. The multi-model ensemble mean of the one standard deviation from each model was calculated lastly.

References

- Bintanja R, Van der Linden E. 2013. The changing seasonal climate in the Arctic. *Sci. Rep.* **3**: 1–8, doi: 10.1038/srep01556.
- Chen X, Tung K-K. 2014. Varying planetary heat sink led to global-warming slowdown and acceleration. *Science* **345**: 897–903.
- Cohen J, Screen JA, Furtado JC, Barlow M, Whittleston D, Coumou D, Francis J, Dethloff K, Entekhabi D, Overland J. 2014. Recent Arctic amplification and extreme mid-latitude weather. *Nat. Geosci.* **7**: 627–637.
- Deser C, Phillips A, Bourdette V, Teng H. 2012. Uncertainty in climate change projections: the role of internal variability. *Clim. Dyn.* **38**: 527–546.
- England MH, McGregor S, Spence P, Meehl GA, Timmermann A, Cai W, Gupta AS, McPhaden MJ, Purich A, Santoso A. 2014. Recent intensification of wind-driven circulation in the Pacific and the ongoing warming hiatus. *Nat. Clim. Change* **4**: 222–227.
- Fletcher CG, Zhao H, Kushner PJ, Fernandes R. 2012. Using models and satellite observations to evaluate the strength of snow albedo feedback. *J. Geophys. Res. Atmos.* **117**: D11117, doi: 10.11029/12012JD017724.
- Fu Q, Johanson CM, Wallace JM, Reichler T. 2006. Enhanced mid-latitude tropospheric warming in satellite measurements. *Science* **312**: 1179.
- Guemas V, Doblas-Reyes FJ, Andreu-Burillo I, Asif M. 2013. Retrospective prediction of the global warming slowdown in the past decade. *Nat. Clim. Change* **3**: 649–653.
- Hansen J, Ruedy R, Sato M, Lo K. 2010. Global surface temperature change. *Rev. Geophys.* **48**: RG4004.
- Harris I, Jones P, Osborn T, Lister D. 2013. Updated high resolution grids of monthly climatic observations—the CRU TS3.10 Dataset. *Int. J. Climatol.* **34**: 623–642.
- Hassanzadeh P, Kuang Z, Farrell BF. 2014. Responses of midlatitude blocks and wave amplitude to changes in the meridional temperature gradient in an idealized dry GCM. *Geophys. Res. Lett.* **41**: 5223–5232.
- He Y, Huang J, Ji M. 2014. Impact of land–sea thermal contrast on interdecadal variation in circulation and blocking. *Clim. Dyn.* **43**: 3267–3279, doi: 10.1007/s00382-00014-02103-y.
- Higuchi K, Huang J, Shabbar A. 1999. A wavelet characterization of the North Atlantic oscillation variation and its relationship to the North Atlantic sea surface temperature. *Int. J. Climatol.* **19**: 1119–1129.
- Huang J, Guan X, Ji F. 2012. Enhanced cold-season warming in semi-arid regions. *Atmos. Chem. Phys.* **12**: 5391–5398.
- Huang J, Higuchi K, Shabbar A. 1998. The relationship between the North Atlantic Oscillation and El Niño–Southern Oscillation. *Geophys. Res. Lett.* **25**: 2707–2710.
- Huang JP, Ji MX, Higuchi K, Shabbar A. 2006. Temporal structures of the North Atlantic Oscillation and its impact on the regional climate variability. *Adv. Atmos. Sci.* **23**: 23–32.
- Huang J, Yu H, Guan X, Wang G, Guo R. 2015. Accelerated dry-land expansion under climate change. *Nat. Clim. Change* 1–7, doi: 10.1038/nclimate2837.
- IPCC. 2007. Summary for Policymakers. In: *Climate Change 2007: The Physical Science Basis*. Contribution of Working Group I to the Fourth Assessment Report of the Intergovernmental Panel on Climate Change, Solomon S, Qin D, Manning M, Chen Z, Marquis M, Averyt KB, Tignor M, Miller HL (eds). Cambridge University Press: Cambridge, UK and New York, NY, 1–18.
- Jeong JH, Ou T, Linderholm HW, Kim BM, Kim SJ, Kug JS, Chen D. 2011. Recent recovery of the Siberian high intensity. *J. Geophys. Res. Atmos.* **116**: D23102, doi: 10.21029/22011JD015904.
- Ji F, Wu Z, Huang J, Chassignet EP. 2014. Evolution of land surface air temperature trend. *Nat. Clim. Change* **4**: 462–466, doi: 10.1038/nclimate2223.
- Jones P, Lister D, Osborn T, Harpham C, Salmon M, Morice C. 2012. Hemispheric and large scale land surface air temperature variations: an extensive revision and an update to 2010. *J. Geophys. Res. Atmos.* **117**: D05127, doi: 10.101029/2011JD017139.
- Joshi MM, Gregory JM, Webb MJ, Sexton DM, Johns TC. 2008. Mechanisms for the land/sea warming contrast exhibited by simulations of climate change. *Clim. Dyn.* **30**: 455–465.
- Kosaka Y, Xie S-P. 2013. Recent global-warming hiatus tied to equatorial Pacific surface cooling. *Nature* **501**: 403–407.
- Lawrimore JH, Menne MJ, Gleason BE, Williams CN, Wuertz DB, Vose RS, Rennie J. 2011. An overview of the Global Historical Climatology Network monthly mean temperature data set, version 3. *J. Geophys. Res. Atmos.* **116**: D19121, doi: 10.11029/12011JD016187.
- Li F, Wang H, Liu J. 2014. The strengthening relationship between Arctic Oscillation and ENSO after the mid 1990s. *Int. J. Climatol.* **34**: 2515–2521.
- Liu J, Zhang Z, Inoue J, Horton RM. 2007. Evaluation of snow/ice albedo parameterizations and their impacts on sea ice simulations. *Int. J. Climatol.* **27**: 81–91.
- Liu Y, Huang J, Shi G, Takamura T, Khatri P, Bi J, Shi J, Wang T, Wang X, Zhang B. 2011. Aerosol optical properties and radiative effect determined from sky-radiometer over Loess Plateau of Northwest China. *Atmos. Chem. Phys.* **11**: 11455–11463.

- Lorantý MM, Berner LT, Goetz SJ, Jin Y, Randerson JT. 2014. Vegetation controls on northern high latitude snow albedo feedback: observations and CMIP5 model simulations. *Global Change Biol.* **20**: 594–606.
- McCabe GJ, Ault TR, Cook BI, Betancourt JL, Schwartz MD. 2012. Influences of the El Niño Southern Oscillation and the Pacific Decadal Oscillation on the timing of the North American spring. *Int. J. Climatol.* **32**: 2301–2310.
- Mori M, Watanabe M, Shiogama H, Inoue J, Kimoto M. 2014. Robust Arctic sea-ice influence on the frequent Eurasian cold winters in past decades. *Nat. Geosci.* **7**: 869–873.
- Morice CP, Kennedy JJ, Rayner NA, Jones PD. 2012. Quantifying uncertainties in global and regional temperature change using an ensemble of observational estimates: the HadCRUT4 data set. *J. Geophys. Res. Atmos.* **117**: 1–22, doi: 10.1029/2011JD017187.
- Overland JE, Spillane MC, Percival DB, Wang M, Mofjeld HO. 2004. Seasonal and regional variation of pan-Arctic surface air temperature over the instrumental record. *J. Clim.* **17**: 3263–3282.
- Pithan F, Mauritsen T. 2014. Arctic amplification dominated by temperature feedbacks in contemporary climate models. *Nat. Geosci.* **7**: 181–184, doi: 10.1038/NNGEO2071.
- Rayner NA, Parker DE, Horton EB, Folland CK, Alexander LV, Rowell DP, Kent EC, Kaplan A. 2003. Global analyses of sea surface temperature, sea ice, and night marine air temperature since the late nineteenth century. *J. Geophys. Res. Atmos.* **108**(D14): 1–37, doi: 10.1029/2002JD002670.
- Screen JA, Simmonds I. 2010. The central role of diminishing sea ice in recent Arctic temperature amplification. *Nature* **464**: 1334–1337.
- Shabbar A, Huang J, Higuchi K. 2001. The relationship between the wintertime North Atlantic Oscillation and blocking episodes in the North Atlantic. *Int. J. Climatol.* **21**: 355–369.
- Smith TM, Reynolds RW, Peterson TC, Lawrimore J. 2008. Improvements to NOAA's historical merged land-ocean surface temperature analysis (1880–2006). *J. Clim.* **21**: 2283–2296.
- Taylor KE, Stouffer RJ, Meehl GA. 2012. An overview of CMIP5 and the experiment design. *Bull. Am. Meteorol. Soc.* **93**: 485–498.
- Thompson DW, Wallace JM. 2000. Annular modes in the extratropical circulation. Part I: month-to-month variability*. *J. Clim.* **13**: 1000–1016.
- Trenberth K, Jones P, Ambenje P, Bojariu R, Easterling D, Klein T, Parker D, Renwick J, Rusticucci M, Soden B. 2007. Observations: surface and atmospheric climate change. In *In Climate Change 2007: The Physical Science Basis*. Contribution of Working Group I to the Fourth Assessment Report of the Intergovernmental Panel on Climate Change, Solomon S, Qin D, Manning M, Chen Z, Marquis M, Averyt K, Tignor M, Miller H (eds). Cambridge University Press: Cambridge, UK and New York, NY, 237–253.
- Wallace JM, Fu Q, Smoliak BV, Lin P, Johanson CM. 2012. Simulated versus observed patterns of warming over the extratropical Northern Hemisphere continents during the cold season. *Proc. Natl. Acad. Sci.* **109**: 14337–14342.
- Wang M, Overland JE. 2004. Detecting Arctic climate change using Köppen climate classification. *Clim. Change* **67**: 43–62.
- Wang W-C, Stone PH. 1980. Effect of ice-albedo feedback on global sensitivity in a one-dimensional radiative-convective climate model. *J. Atmos. Sci.* **37**: 545–552.